esa

ECOSPHERE

CONCEPTS & THEORY

Prototype campaign assessment of disturbance-induced tree loss effects on surface properties for atmospheric modeling

Juan Camilo Villegas,[1,2,]† Darin J. Law,[2] Scott C. Stark,[3] David M. Minor,[3] David D. Breshears,[2,4] Scott R. Saleska,[4] Abigail L. S. Swann,[5,6] Elizabeth S. Garcia,[6] Elizabeth M. Bella,[7,8] John M. Morton,[8] Neil S. Cobb,[9] Greg A. Barron-Gafford,[10] Marcy E. Litvak,[11] and Thomas E. Kolb[9,12]

[1]*Grupo GIGA, Escuela Ambiental, Universidad de Antioquia, Apartado Aéreo 1226, Medellín, Colombia*
[2]*School of Natural Resources and the Environment, University of Arizona, Tucson, Arizona 85721 USA*
[3]*Department of Forestry, Michigan State University, East Lansing, Michigan 48824 USA*
[4]*Department of Ecology and Evolutionary Biology, University of Arizona, Tucson, Arizona 85721 USA*
[5]*Department of Biology, University of Washington, Seattle, Washington 98195 USA*
[6]*Department of Atmospheric Sciences, University of Washington, Seattle, Washington 98195 USA*
[7]*AECOM, Anchorage, Alaska 99501 USA*
[8]*Kenai National Wildlife Refuge, U.S. Fish and Wildlife Service, Soldotna, Alaska 99669 USA*
[9]*Merriam-Powell Center for Environmental Research, Northern Arizona University, Flagstaff, Arizona 86011 USA*
[10]*School of Geography and Regional Development, University of Arizona, Tucson, Arizona 85721 USA*
[11]*Department of Biology, University of New Mexico, Albuquerque, New Mexico 87131 USA*
[12]*School of Forestry, Northern Arizona University, Flagstaff, Arizona 86011 USA*

Citation: Villegas, J. C., D. J. Law, S. C. Stark, D. M. Minor, D. D. Breshears, S. R. Saleska, A. L. S. Swann, E. S. Garcia, E. M. Bella, J. M. Morton, N. S. Cobb, G. A. Barron-Gafford, M. E. Litvak, and T. E. Kolb. 2017. Prototype campaign assessment of disturbance-induced tree loss effects on surface properties for atmospheric modeling. Ecosphere 8(3): e01698. 10.1002/ecs2.1698

Abstract. Changes in large-scale vegetation structure triggered by processes such as deforestation, wildfires, and tree die-off alter surface structure, energy balance, and associated albedo—all critical for land surface models. Characterizing these properties usually requires long-term data, precluding characterization of rapid vegetation changes such as those increasingly occurring in the Anthropocene. Consequently, the characterization of rapid events is limited and only possible in a few specific areas. We use a campaign approach to characterize surface properties associated with vegetation structure. In our approach, a profiling LiDAR and hemispherical image analyses quantify vegetation structure and a portable mast instrumented with a net radiometer, wind–humidity–temperature stations in a vertical profile, and soil temperature–heat flux characterize surface properties. We illustrate the application of our approach in two forest types (boreal and semiarid) with disturbance-induced tree loss. Our prototype characterizes major structural changes associated with tree loss, changes in vertical wind profiles, surface roughness energy balance partitioning, a proxy for NDVI (Normalized Differential Vegetation Index), and albedo. Multi-day albedo estimates, which differed between control and disturbed areas, were similar to tower-based multi-year characterizations, highlighting the utility and potential of the campaign approach. Our prototype provides general characterization of surface and boundary-layer properties relevant for land surface models, strategically enabling preliminary characterization of rapid vegetation disturbance events.

Key words: albedo; energy balance; tree die-off; vegetation disturbance; vegetation structure.

Received 21 December 2016; accepted 22 December 2016. Corresponding Editor: Debra P. C. Peters.

† **E-mail:** camilo.villegas@udea.edu.co

Introduction

Vegetative structure fundamentally affects the exchange of energy and momentum between the surface and the atmosphere as well as the partitioning of energy flux between components of the surface radiation budget. Vegetation change can thus alter radiation balance partitioning via surface properties such as albedo—the proportion of incident shortwave (SW) radiation that is reflected to the atmosphere. Along with potential modifications of SW energy balance, changes in surface properties may also induce changes in the longwave (LW) radiation balance (Liu et al. 2005, Baldocchi and Ma 2013). Large-scale vegetation structure change can, therefore, alter near-surface energy availability (net radiation) and its partitioning into latent and sensible heat components. Latent and sensible heat flux partitioning is also affected by the availability of soil moisture and the ecophysiological characteristics of vegetation, which are also altered by vegetation change (Villegas et al. 2014). Additionally, vegetation change alters surface turbulence by changing the three-dimensional structure and thus roughness of the canopy. Turbulence, in turn, alters boundary-layer properties impacting mass, energy, and momentum exchanges, particularly when tree-dominated landscapes are replaced by more heterogeneous and/or herbaceous cover types leading to a more emissive boundary layer (Bonan 2008, Davin and de Noblet-Ducoudré 2010).

Land use and climate change are driving extensive changes in vegetation. These drivers include managed changes to the land surface such as deforestation as well as climate-driven changes such as tree loss from wildfire, drought-induced die-off, invasive natural enemies, and other factors (Allen et al. 2010, 2015, Williams et al. 2013). The speed and extent at which changes in vegetation are occurring, and their wide geographic distribution pose a challenge for modeling surface–atmosphere responses to vegetation disturbance because, for many disturbed ecosystems, we lack characterization of key surface properties that represent the effects of land surface changes, particularly with respect to the changes in vegetation structural attributes and energy balance partitioning (Running 2008). Consequently, rapid assessment protocols such as those implemented in the past for other purposes (e.g., Anderson and Goulden 2009) are needed to characterize the effects of these disturbances. They are especially needed to advance understanding of ecoclimate teleconnections—ecological changes in one area that influence climate and produce ecological responses in others—which are assessed with broad-scale surface-atmosphere modeling (Stark et al. 2016, Garcia et al. 2016). Characterizing the change in surface properties associated with land surface change usually requires months to years using permanent flux towers (Liu et al. 2005), making it difficult to rapidly assess the effects of abrupt vegetation change. Additionally, such characterizations require paired or gradient sampling—from impacted to non-impacted sites—which is challenging for permanent flux tower installations due to the high resource costs associated with each tower, such that co-located disturbed and undisturbed comparisons are uncommon and hard to achieve (but see Liu et al. 2005, Liu and Randerson 2008).

Additionally, a key dimension of quantifying impacts of vegetation change on surface energy balance is developing strong quantitative links to specific ecological changes. Globally, tree die-off and increased tree mortality range from landscape-scale tree die-off in southwestern North America (Breshears et al. 2005) to moderate increases in the mortality of large trees in the Amazon (Phillips et al. 2009), and are emerging as a climate change-related crisis (Allen et al. 2015). Similarly, wildfires are increasingly altering landscapes (Williams et al. 2013). Linking ecological changes with energy balance impacts is critical to upscale and understand the broad-scale consequences of vegetation change (e.g., McDowell et al. 2016) elsewhere for the climate and for vegetation (Stark et al. 2016).

Here, we describe a campaign approach prototype for characterizing surface attributes associated with vegetation structure and energy balance partitioning that does not require a fully instrumented flux tower and can achieve general characterization of the surface with short-term measurements. Our approach (initially proposed by Stark et al. 2016) compares vegetation impacted by recent disturbance with co-located control vegetation to quantify ecological change and link it with energy balance consequences.

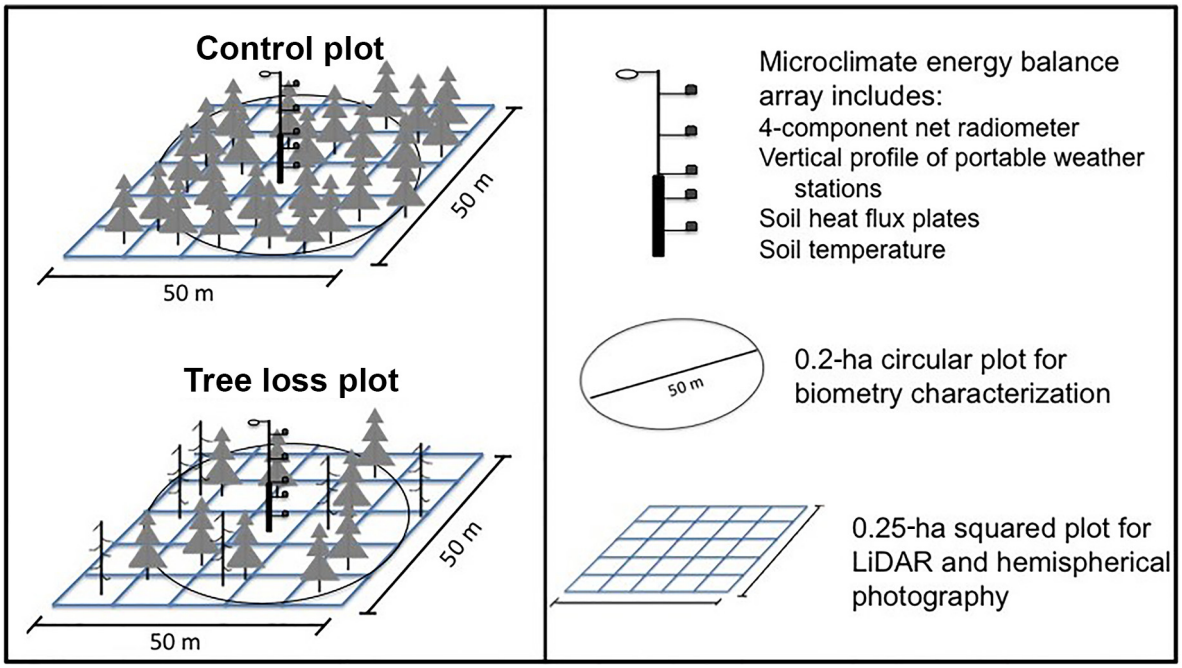

Fig. 1. Campaign assessment experimental setup for assessing the effects of vegetation disturbance on key ecosystem properties affecting ecoclimate teleconnections. Experimental setup includes the installation of a portable mast with microclimate and energy balance instrumentation, and the characterization of tree structural attributes around the footprint of the mast via biometric characterization of vegetation combined with LiDAR profiling and hemispherical photography.

First, we characterize vegetation structure with profiling LiDAR and hemispherical image analyses and with traditional biometry measurements. Next, employing a portable mast instrumented with a four-component net radiometer, a vertical profile of portable wind–humidity–temperature stations, and soil temperature–heat flux sensors, we simultaneously estimate energy balance components, their partitioning, and their response to vegetation change. It focuses on a pair of sites—one of which is more disturbed—precluding the need for space for time substitution in comparing sites. We illustrate the application of this method in two forest types with disturbance-induced tree loss: (1) a boreal forest in Alaska with tree die-off and subsequent wildfire and (2) a semiarid forest in northern Arizona, where tree die-off and selective forest thinning have affected forest structure. We contrast our campaign assessment observations of albedo with long-term tower-based albedo estimates, when applicable.

Methods—Rapid Assessment Prototype

Vegetation structure characterization

Our proposed prototype provides a rapid biometric characterization of all standing stems (both dead and live trees) with diameter at breast height > 1 cm in a 50 m diameter circular plot, centered at the location of the microclimate array (Fig. 1). This plot size was determined by the observational footprint of the four-component net radiometer, located at the center of the plot. Additionally, we established a 50 × 50 m grid (with the microclimate array in the center), with 10-m transects both in north–south and in east–west directions, for LiDAR characterization (covering a total of 12 transects, six in each direction) and hemispherical photography on each transect intersection, for a total of 36 photographs per plot (Fig. 1). Canopy structural attributes were characterized using a profiling LiDAR system that uses a narrow-beam rapidly pulsed first-return laser rangefinder coupled with a data recording system to

quantify vertical vegetation structure from the rate of pulse transmission in 1-m vertical bins (measurements along ~1 m wide transects with a 2-m horizontal bin grain; Parker et al. 2004, Stark et al. 2012, 2016). Additionally, we linked vegetation structure with near-ground solar radiation using hemispherical photographs taken 1 m above the ground with a digital camera with a 180° field-of-view fish-eye lens. We used a standard radiation simulation computational tool (Hemiview canopy analysis software version 2.1; Rich et al. 1999) to calculate the proportion of direct solar radiation that reaches the surface relative to that for an open-sky situation at the same location (direct site factor, DSF) as well as to estimate leaf area index (LAI) for each location (Rich et al. 1999, Royer et al. 2010).

Portable microclimate characterization

At the center of each plot, we installed an 18-m portable mast instrumented with a net radiometer at the top (CNR4 net radiometer, Delft, The Netherlands), collecting five-minute averages of all four components of net radiation (long- and SW upwelling and downwelling components) for a period of 72 h. To complete the radiation balance measurements, a soil heat flux plate was installed at a depth of 10 cm and located 3 m away on the north side of the mast (HFP01 Soil heat flux plate; Campbell Scientific, Logan, Utah, USA). Our estimates from the heat flux plate are affected by soil settling, and the short-term nature of our campaign precludes longer-term soil settling occurring during the measurement interval; however, G is a relatively small component of the energy budget (both specifically in our data and more generally in most site energy balances), so we do not expect this term to have a large effect on our estimate of net radiation. For redundancy, a soil temperature gradient measurement system was co-located with the soil heat flux plate, with two soil thermocouples (107-L temperature probe; Campbell Scientific) installed at 5 and 10 cm depths. An array of portable weather stations (Kestrel weather meter 4500; Nielsen Kellerman, Boothwyn, Pennsylvania, USA. Kestrel 4500 is no longer produced and was replaced by a newer model Kestrel 550 as of 2015) were installed on horizontal arms extending 1 m out of the mast at six heights (1, 3, 5, 10, 15, and 17 m) to characterize wind–humidity–temperature profiles in the near surface, which were later used to estimate Bowen ratio (Fig. 1). This approach is intended for a field campaign that includes a pair of sites—one of which has more disturbance and potentially limited vehicular access—and is inherently less comprehensive than long-term flux measurements, but nonetheless provides a general approximation of structural attributes and energy balance partitioning, such that overall differences between undisturbed and disturbed ecosystems can be estimated.

Energy balance partitioning into sensible and latent heat components was estimated through the combination of net radiation, soil heat flux, and temperature–relative humidity vertical profiles (assuming canopy heat storage is small compared to other fluxes over the campaign timeframe), using the Bowen ratio/energy budget method which assumes that the vertical flows of sensible and latent heat are proportional to vertical gradients of temperature and humidity in the atmosphere in the scale of meters to tens of meters (β—the ratio of sensible to latent heat flux; Shuttleworth 2012). More specifically, we calculate available energy (Rn-G) as the difference between net radiation (Rn—derived from net LW to SW radiation components in the net radiometer) and ground heat flux (G—comparatively small). We then use the Bowen ratio estimate (β—calculated from the measured vertical gradients of virtual potential temperature and vapor pressure) to partition available energy into sensible and latent heat components. We also estimated a proxy for NDVI based on data from the four-component net radiometer, similar to approaches others have used (Huemmrich et al. 1999, Doughty and Goulden 2008):

$$\mathrm{NDVI} = \frac{\mathrm{Albedo\_NIR} - \mathrm{Albedo\_PAR}}{\mathrm{Albedo\_NIR} + \mathrm{Albedo\_PAR}}$$

where NIR and PAR correspond to the near infrared and photosynthetically active radiation portions of the spectrum and are estimated as the SW and LW measurements in the four-component net radiometer, such that:

$$\mathrm{NDVI\_proxy} = \frac{\mathrm{Albedo\_LW} - \mathrm{Albedo\_SW}}{\mathrm{Albedo\_LW} + \mathrm{Albedo\_SW}}.$$

Through a combination of canopy structural and radiative properties described above, we estimate the fraction of absorbed photosynthetically

active radiation (FAPAR; similar to the approach used by Wu et al. 2016):

$$\text{FAPAR} = (1 - \rho_1) - (1 - \rho_2) \times \exp\left(\frac{\alpha \times \text{LAI}}{\cos(\text{SZA})}\right)$$

where ρ_1 is the canopy reflectivity at the top (for which we use our albedo estimate), ρ_2 is the canopy reflectivity at the bottom (for which we use a value of 0.1, based on conifer estimates by Gates et al. 1965), α is the light transmission coefficient (for which we use our DSF values), LAI is the leaf area index (for which we use or hemispherical photography estimates), and SZA is the solar zenith angle (for which we use a value of 0 in both cases).

Results and Discussion

Example applications of prototype from disturbance-induced tree loss

We identified key sites recently impacted by large-scale vegetation disturbance in two dominant North American vegetation types: a white spruce (*Picea glauca*)/Lutz spruce (*Picea* × *Lutzii*)- and paper birch (*Betula neoalaskana*)-dominated boreal system on the Kenai Peninsula in south central Alaska (60.10° N, 151.18° W), where a control forest plot (unimpacted for at least 15 yr) was located adjacent to a recently disturbed forest plot, impacted by tree mortality and wildfire. In this location, disturbance was associated with tree die-off caused by a combination of an extensive spruce bark beetle outbreak (Berg et al. 2006) and changing wildfire regime (Berg and Anderson 2006, Morton et al. 2006). Similarly, we established an experimental contrast in two semiarid conifer forest plots dominated by ponderosa pine (*Pinus ponderosa*) with occurrence of other conifer species, as well as Gambel's oak (*Quercus gambelii*), northern Arizona (35.14° N, 111.73° W). In this area, tree cover was lost due to a combination of die-off occurring within the last decade, combined with management practices aimed at fire management (thinning).

The biometric observations in areas of contrasting tree disturbance show major structural changes from ecological change, reflected by differences in tree size distributions (Fig. 2A, B). The disturbed boreal forest plot shows (Fig. 2A) a similar relative shape of the size distribution histogram, yet with frequency of trees at all sizes decreased relative to the control. By contrast, in the semiarid forest, the relative size distribution shows a loss of relatively large trees in the disturbed plot where disturbance was associated with die-off (Fig. 2B). Vertical canopy profiles obtained from LiDAR scans reflect these patterns in both forests (Fig. 2C, D). More specifically, there was a general reduction in foliar density in the boreal forest, yet the vertical structure of the forest was maintained (Fig. 2C). In contrast, the change in tree size distribution was related to an overall change in vertical vegetation structure in the semiarid forest, where the loss of large trees shifts the peak in foliar density to a lower height in the canopy (Fig. 2D).

Vegetation disturbance is also illustrated by increased values of the DSF derived from hemispherical photography for both impacted plots when compared to their controls (Mann–Whitney rank sum test $P < 0.001$; Fig. 3A, B). Notably, this effect is more pronounced in the semiarid forest where the type of disturbance leads to a much lower proportion of remaining standing vegetation in the plot, as highlighted by the structural change after disturbance (Fig. 2B). In contrast, for the lower-density boreal system, a greater proportion of standing dead trees was present, potentially contributing to increased radiation interception, which led to less pronounced differences between the control and disturbed plots (Fig. 3B). Similarly, LAI estimates from hemispherical photography reflected the effect of vegetation disturbance with significant decreases in both the boreal (Fig. 3C) and semiarid forests (Fig. 3D). Fraction of absorbed photosynthetically active radiation estimates (Fig. 3E, F) reflect the open nature of both systems, characterized by high values of canopy transmittance (indicated by DSF) and low values of LAI, resulting in low values of FAPAR that drop to almost zero in the disturbed plots. These values reflect the condition of the tree canopy and not the entire ecosystem, including the understory (hemispherical photography estimates used in the calculation do not account for herbaceous or small statured vegetation near the ground), highlighting the potentially significant alterations in ecosystem dynamics immediately after tree disturbance, when understory vegetation has not responded.

Tree cover loss induces a change in vertical wind profiles (Fig. 4A, B), decreasing surface

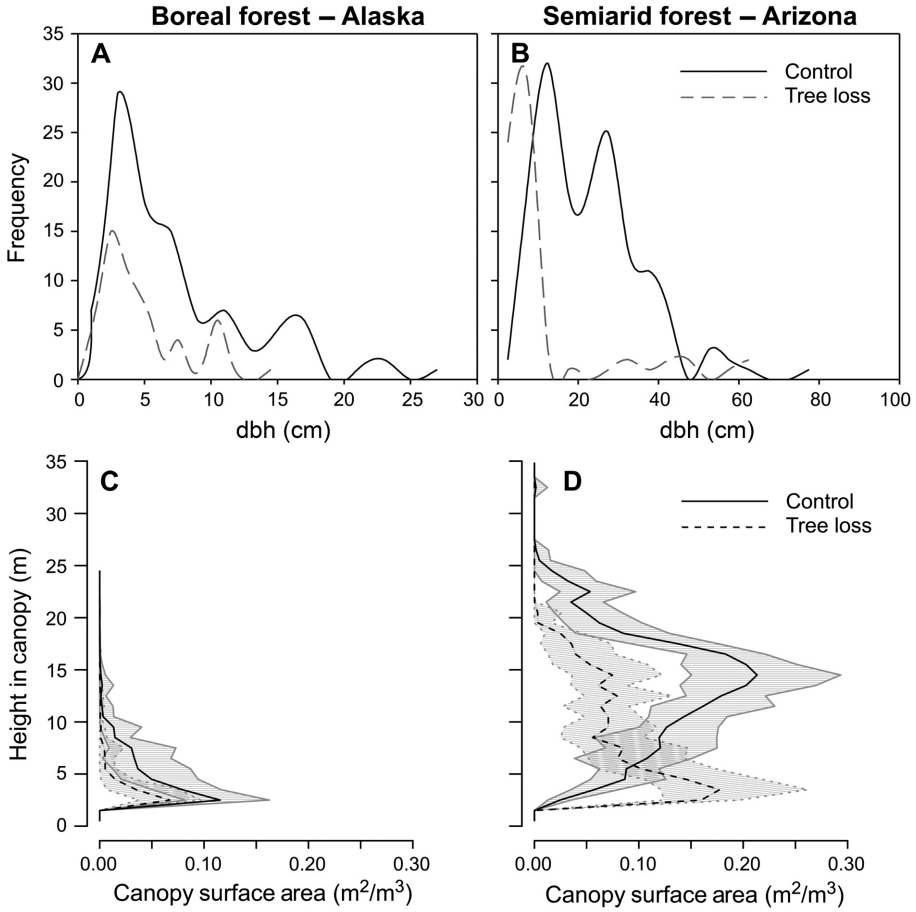

Fig. 2. Detailed structural characterization of vegetation via biometric measurements for (A) boreal forest contrast and (B) semiarid conifer forest contrast, including diameter at breast height (dbh) metrics in contrast to control and tree loss plots; LiDAR characterization (C, boreal, D, semiarid).

roughness and affecting surface characteristics that determine the potential for surface–atmosphere exchange of mass and energy. Decreased roughness is more evident in the boreal forest, compared with the semiarid forest, and is associated with a more extensive disturbance impact and a more disperse canopy after disturbance (as highlighted by canopy structural attributes, Fig. 2). Additionally, as canopy density and height are generally greater in the semiarid forest (Fig. 2D), roughness length is also generally greater, even in disturbed locations. This leads to more pronounced canopy effects on wind speed and results in smaller differences between control and disturbed locations. Further application of our proposed prototype would allow derivation of structure–roughness relationships useful for improving prediction of surface processes associated with energy and mass exchange (Menenti and Ritchie 1994, Lefsky et al. 2002).

The mean daily cycle of available energy (as quantified by "Rn-*G*"—net radiation Rn minus ground heat flux *G*) did not vary significantly between disturbed and undisturbed plots in the boreal forest (Fig. 4C), potentially due to similar amounts of open understory with similar cover in both locations, as well as the influence of dead standing trees on vegetation structure. In contrast, the mean daily cycle of available energy in the semiarid forest showed lower available energy in the disturbed plot, compared to the control, during the daytime hours. This is due to higher values of outgoing radiation (in both short- and LW portions of the spectrum) and

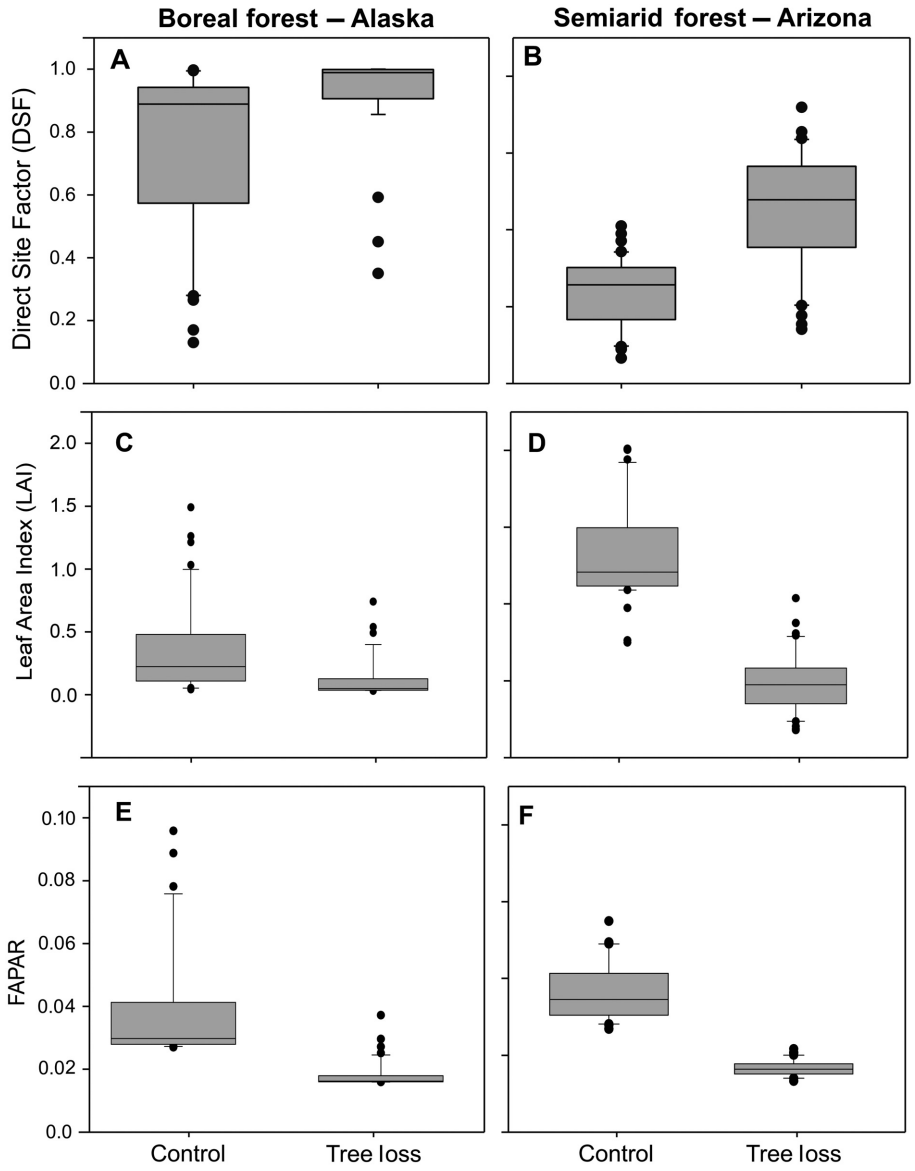

Fig. 3. Estimation of canopy effects on incoming solar radiation as illustrated by direct site factor (DSF; proportion of annual direct solar radiation that reaches the surface relative to that for an open-sky situation at the same location) in (A) boreal and (B) semiarid; leaf area index (LAI) for boreal (C) and semiarid (D) forest contrasts; and fraction of absorbed photosynthetically active radiation (FAPAR) for boreal (E) and semiarid (F) forest contrasts.

greater heat dissipation to the ground in the disturbed plot (Fig. 4D). The trend is reversed during the night hours, when the emission of LW radiation is greater in the more open-disturbed site compared to the control.

Despite the contrast in total available energy, vegetation activity does not significantly vary between control and disturbed plots for both forest types, as highlighted by our NDVI proxy. There is a slight decrease in NDVI_proxy values after disturbance for the semiarid forest, whereas in the boreal system a slight increase in this metric was recorded (Fig. 4E, F). Likely most vegetation activity is associated with understory vegetation as canopy FAPAR values (Fig. 3E, F) were considerably low. Consequently, there were

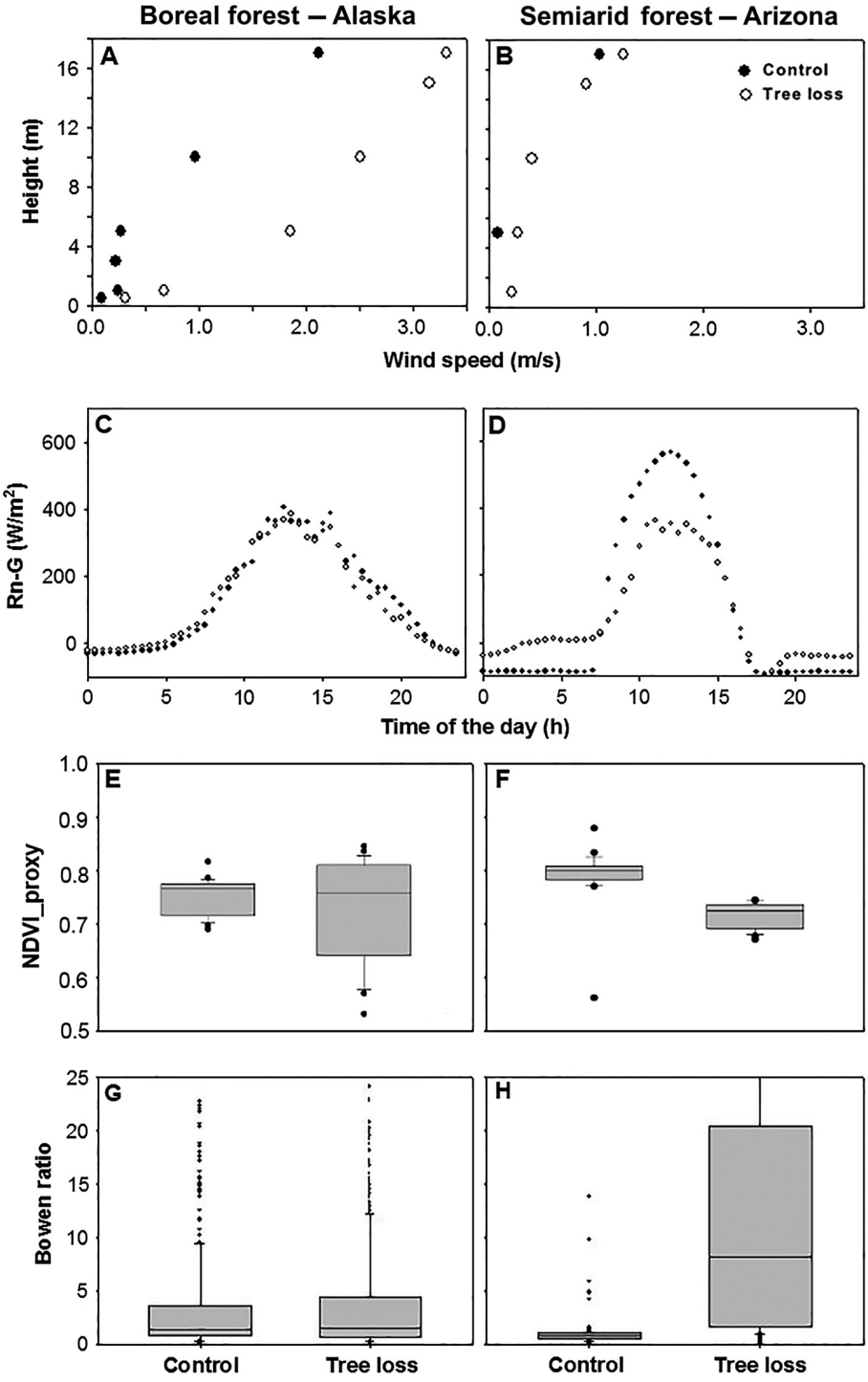

Fig. 4. Characterization of forest disturbance effects on surface properties as illustrated by changes in wind speed profiles for (A) boreal forest contrast and (B) semiarid forest contrast; daily cycle of available net radiation (difference between net radiation and ground heat flux) for (C) boreal and (D) semiarid forest contrast; NDVI_proxy for boreal (E) and (F) semiarid; and energy balance partitioning as illustrated by Bowen ratio for (G) boreal and (H) semiarid forest.

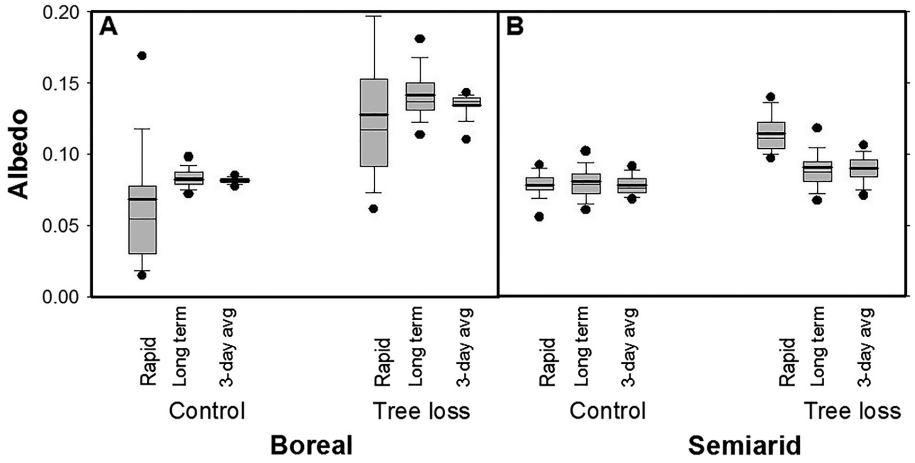

Fig. 5. Comparison of albedo values derived from campaign assessment prototype (rapid) with long-term observations from eddy covariance measurements (long term) and three-day running averages from the long-term data (3-day avg) for (A) boreal forest and (B) semiarid forest. Campaign assessment estimates are not significantly different from long-term estimates (Mann–Whitney rank sum test with significance at ≤0.1), except in the case of tree loss observations for semiarid forest, where long-term estimates were derived from a reference site with different characteristics. Three-day running means are not significantly different from long-term mean values.

no significant differences in the partitioning of available energy into sensible and latent heat components between control and disturbed plots. This was particularly evident in the boreal forest, as illustrated by the distribution of values in the Bowen ratio (Fig. 4G, H). In both the boreal and semiarid systems, however, there is higher variability in Bowen ratio values in disturbed locations, compared to the control sites, which is related to higher spatial variability in vegetation cover and associated meteorological changes in the height profiles noted previously.

To further illustrate the utility of our proposed approach to characterize model-relevant landscape properties, we compared our multi-day estimates of albedo against multi-year characterizations from Ameriflux sites. Albedo is a surface property that defines key components of surface–atmosphere interactions at these locations, and has particularly important implications for defining ecoclimate teleconnections (Randerson et al. 2006, Swann et al. 2012, Stark et al. 2016). For the boreal forest, we extracted daytime albedo values (8:00–18:00) for a climatically comparable period (June, July, August) in a three-year record for a fire chronosequence (2002–2004), with characteristics like those in our study sites (Delta Junction 1920 burn Alaska, USA, 63.89° N, 145.74° W; Delta Junction 1999 burn, Alaska, USA, 63.92° N, 145.75° W; Liu et al. 2005). In the semiarid forest, we extracted daytime albedo records (8:00–17:00) for August-October 2005–2010 at the "Flagstaff unmanaged forest" site (35.09° N, 111.76° W), corresponding to the base condition, and the "Flagstaff managed forest" corresponding to the disturbed location (35.14° N, 111.73° W). Overall, our observed albedo values did not differ significantly from the long-term values (Fig. 5), except for the disturbed semiarid forest. In this case, albedo was lower at the long-term flux site, where tree density was lowered due to thinning as opposed to die-off, making it a less direct proxy to our campaign site where tree die-off was the primary driver of lowered tree density. To further assess the potential for using short-term measurements of albedo as an estimate of longer-term estimates, we calculated 72-h average daytime albedo values from the long-term data set at all four tower locations and compared them with three-day averages from the same data set. The mean albedo values for these two periods collected from the same flux tower did not significantly different from each other (Fig. 5). Collectively, these results highlight the utility of our proposed rapid approach for characterization of vegetation disturbance effects on landscape properties.

Potential campaign approach application

We have prototyped a previously proposed campaign approach for assessing the effect of vegetation disturbance on general processes linking surface–atmosphere dynamics that are particularly relevant to regional-to-global ecoclimatic dynamics (Stark et al. 2016). Notably, our campaign approach provides a general characterization of surface and boundary-layer properties relevant for models of vegetation-mediated surface–atmosphere exchange at a relatively low cost and without the requirement of multi-year observations. This approach is intended to complement—rather than to replace—characterization of surface–atmosphere properties by enabling timely sampling of more vegetation types and disturbance regimes in otherwise unsuitable conditions. More specifically, it complements permanent tower locations, enabling less logistically constrained characterization of multiple vegetation states, including gradients of vegetation disturbance and/or the effects of disturbance on surface properties for different seasons. In contrast to previous campaign approaches (e.g., Anderson and Goulden 2009), our approach has continuous measurements as opposed to individual measurements at different times; this allows us direct estimation of disturbance effects rather than space for time substitutions. We were able to document changes from tree die-off alone or with wildfire following some vegetation recovery; we expect the approach would readily detect even larger changes such as those immediately after wildfire. Further development of our proposed approach is expected to lead to a more robust, generally applicable, and cost- and time-efficient approach for general characterization of the effects of vegetation transformation. Our approach can potentially be further enhanced as needed by including additional instrumentation such as water vapor analyzers and 3D sonic anemometers, as well as a more refined measurement of ground heat fluxes. Importantly, our approach provides empirical estimates of input parameters critical to land surface models, including albedo and LAI, and provides proxy metrics for characterizing disturbance impacts such as NDVI and FAPAR. These can be useful for considering how to scale from points up to the larger-scale resolution of land surface models. Our results can be scaled up to the grid cells of land surface models by using ratios of disturbed/undisturbed as applied to the proportion of disturbed areas (like the approach used in the MODIS Disturbance Index; Mildrexler et al. 2009; e.g., for the semiarid forest example: DSF: 1.48; LAI: 0.46; NDVI: 0.91; Albedo: 1.38; FAPAR: 0.41; for the boreal forest example: DSF: 1.23; LAI: 0.29; NDVI: 1.04; Albedo: 1.71; FAPAR: 0.52). More generally, approaches like the one we propose here are needed to address ecological applications related to ongoing and future rapid vegetation changes and their consequences for site microclimates, land surface–atmospheric feedbacks and ecoclimate teleconnections, and related estimates and management of biogeochemical processes, including carbon accounting.

Acknowledgments

This work was supported primarily through NSF EF-1340624, EF-1340649, and EF-1340604; additional support was provided by Arizona Agricultural Experiment Station, and Estrategia de Sostenibilidad 2014–2015 Universidad de Antioquia. Additional support provided by NSF EF-1550641, EF-1550686, EF-1550756. Data for the northern Arizona sites were funded from grants from the North American Carbon Program/USDA CREES NRI (2004-35111-15057 and 2008-35101-19076) and Science Foundation Arizona (CAA 0-203-08) to T. Kolb at Northern Arizona University. We thank James T. Randerson for data on Alaska boreal forest, obtained directly from Ameriflux database.

Literature Cited

Allen, C. D., D. D. Breshears, and N. G. McDowell. 2015. On underestimation of global vulnerability to tree mortality and forest die-off from hotter drought in the Anthropocene. Ecosphere 6:1–55.

Allen, C. D., et al. 2010. A global overview of drought and heat- induced tree mortality reveals emerging climate change risks for forests. Forest Ecology and Management 259:660–684.

Anderson, R. G., and M. L. Goulden. 2009. A mobile platform to constrain regional estimates of evapotranspiration. Agricultural and Forest Meteorology 149:771–782.

Baldocchi, D., and S. Ma. 2013. How will land use affect air temperature in the surface boundary layer? Lessons learned from a comparative study on the energy balance of an oak savanna and annual grassland in California, USA. Tellus Series B 65:19994.

Berg, E. E., and R. S. Anderson. 2006. Fire history of white and Lutz spruce forests on the Kenai

Peninsula, Alaska, over the last two millennia as determined from soil charcoal. Forest Ecology and Management 227:275–283.

Berg, E. E., J. D. Henry, C. L. Fastie, A. D. DeVolder, and S. M. Matsuoka. 2006. Spruce beetle outbreaks on the Kenai Peninsula, Alaska, and Kluane National Park and Reserved, Yukon Territory: relationship to summer temperatures and regional differences in disturbance regimes. Forest Ecology and Management 227:219–232.

Bonan, G. B. 2008. Forests and climate change: forcings, feedbacks, and the climate benefits of forests. Science 320:1444–1449.

Breshears, D. D., et al. 2005. Regional vegetation die-off in response to global-change-type drought. Proceedings of the National Academy of Sciences USA 102:15144–15148.

Davin, E. L., and N. de Noblet-Ducoudré. 2010. Climatic impact of global-scale deforestation: radiative versus non-radiative processes. Journal of Climate 23:97–112.

Doughty, C. E., and M. L. Goulden. 2008. Seasonal patterns of tropical forest leaf area index and CO_2 exchange. Journal of Geophysical Research 113:G00B06.

Garcia, E., et al. 2016. Synergistic ecoclimate teleconnections from forest loss in different regions structure global ecological responses. PloS ONE 11: e0165042.

Gates, D. M., E. C. Tibbals, and F. Kreith. 1965. Radiation and convection for ponderosa pine. American Journal of Botany 52:66–71.

Huemmrich, K. F., T. A. Black, P. G. Jarvis, J. H. McCaughey, and F. G. Hall. 1999. High temporal resolution NDVI phenology from micrometeorological radiation sensors. Journal of Geophysical Research 104:27935–27944.

Lefsky, M. A., W. B. Cohen, G. G. Parker, and D. J. Harding. 2002. Lidar remote sensing for ecosystem studies. BioScience 52:19–30.

Liu, H., and J. T. Randerson. 2008. Interannual variability of surface energy exchange depends on stand age in a boreal forest fire chronosequence. Journal of Geophysical Research 113:G01006.

Liu, H., J. T. Randerson, J. Lindfors, and F. S. Chapin III. 2005. Changes in the surface energy budget after fire in boreal ecosystems of interior Alaska: an annual perspective. Journal of Geophysical Research 110:D13101.

McDowell, N. G., et al. 2016. Multi-scale predictions of massive conifer mortality due to chronic temperature rise. Nature Climate Change 6:295–300.

Menenti, M., and J. C. Ritchie. 1994. Estimation of effective aerodynamic roughness of Walnut Gulch Watershed with laser altimeter measurements. Water Resources Research 30:1329–1337.

Mildrexler, D. J., M. Zhao, and S. W. Running. 2009. Testing a MODIS Global Disturbance Index across North America. Remote Sensing of Environment 113:2103–2117.

Morton, J. M., E. Berg, D. Newbould, D. MacLean, and L. O'Brien. 2006. Wilderness fire stewardship on the Kenai National Wildlife Refuge, Alaska. International Journal of Wilderness 12:14–17.

Parker, G. G., D. J. Harding, and M. L. Berger. 2004. A portable LIDAR system for rapid determination of forest canopy structure. Journal of Applied Ecology 41:755–767.

Phillips, O. L., et al. 2009. Drought sensitivity of the Amazon rainforest. Science 323:1344–1347.

Randerson, J. T., et al. 2006. The impact of boreal forest fire on climate warming. Science 314:1130–1132.

Rich, P. M., J. Wood, D. A. Vieglais, K. Burek, and N. Webb. 1999. Guide to HemiView: software for analysis of hemispherical photography, manual. Delta-T Devices, Cambridge, UK.

Royer, P. D., D. D. Breshears, C. B. Zou, N. S. Cobb, and S. A. Kurc. 2010. Ecohydrological energy inputs in semiarid coniferous gradients: responses to management-and drought-induced tree reductions. Forest Ecology and Management 260:1646–1655.

Running, S. W. 2008. Ecosystem disturbance, carbon and climate. Science 321:652–653.

Shuttleworth, W. J. 2012. Terrestrial hydrometeorology. Wiley, Chichester, UK.

Stark, S. C., V. Leitold, J. L. Wu, B. J. Enquist, S. R. Saleska, J. Schietti, M. Longo, L. F. Alves, P. B. Camargo, and R. C. Oliveira. 2012. Amazon forest carbon dynamics predicted by profiles of canopy leaf area and light environment. Ecology Letters 15:1406–1414.

Stark, S. C., et al. 2016. Toward accounting for ecoclimate teleconnections: intra- and inter-continental consequences of altered energy balance after vegetation change. Landscape Ecology 31:181–194.

Swann, A. L. S., I. Y. Fung, and J. C. H. Chiang. 2012. Mid-latitude afforestation shifts general circulation and tropical precipitation. Proceedings of the National Academy of Sciences USA 109:712–716.

Villegas, J. C., J. E. Espeleta, C. T. Morrison, D. D. Breshears, and T. E. Huxman. 2014. Factoring in canopy cover heterogeneity on evapotranspiration partitioning: beyond big-leaf surface homogeneity assumptions. Journal of Soil and Water Conservation 69:78A–83A.

Williams, A. P., et al. 2013. Temperature as a potent driver of regional forest drought stress and tree mortality. Nature Climate Change 3:292–297.

Wu, J., et al. 2016. Leaf development and demography explain photosynthetic seasonality in Amazon evergreen forests. Science 351:972–976.